Nuclear Materials and Energy 29 (2021) 101058

Contents lists available at ScienceDirect

Nuclear Materials and Energy

journal homepage: www.elsevier.com/locate/nme

Multiphysics Optimization for First Wall Design Enhancement in Water-Cooled Breeding Blankets

Ruggero Forte [a,*], Pierluigi Chiovaro [a], Pietro Alessandro Di Maio [a], Nasr Ghoniem [b]

[a] Dipartimento di Ingegneria, Università di Palermo, Viale delle Scienze, 90128 Palermo, Italy
[b] Department of Mechanical and Aerospace Engineering, University of California Los Angeles, Los Angeles, CA 90095, United States

ARTICLE INFO

Keywords:
Breeding blanket
Optimization
Complex method
Multiphysics
Neutronics
Thermomechanics

ABSTRACT

The commercial feasibility of the first fusion power plant generation adopting D-T plasma is strongly dependent upon the self-sustainability in terms of tritium fuelling. Within such a kind of reactor, the component selected to house the tritium breeding reactions is the breeding blanket, which is further assigned to heat power removal and radiation shielding functions. As a consequence of both its role and position, the breeding blanket is heavily exposed to both surface and volumetric heat loads and, hence, its design requires a typical multiphysics approach, from the neutronics to the thermo-mechanics. During last years, a great deal of effort has been put in the optimization of the breeding blanket design, with the aim of maximizing the tritium breeding and heat removal performances without undermining its structural integrity. In this paper, a derivative-free optimization method named "Complex method" is applied for the design optimization of the European DEMO Water-Cooled Lithium Lead breeding blanket concept. To this purpose, a potential performances-based objective function, focusing on the maximization of the tritium breeding, is defined and a multiphysics numerical model of the blanket is developed in order to solve the coupled thermo-mechanical problem, while the optimization algorithm leads the design towards a minimum optimum point compliant with the prescribed requirements. Once the optimized design is obtained, its nuclear and thermo-structural performances are assessed by means of specific neutron transport and multiphysics simulations, respectively. Finally, the structural integrity is verified by means of the application of the RCC-MRx design criteria.

1. Introduction

The design of a rational, functional Breeding Blanket (BB) able to guarantee the tritium self-sufficiency of the plant is a pivotal requirement for any next-step nuclear fusion facility beyond ITER [1].

Worldwide, BB concepts are substantially being designed as helium-cooled or water-cooled. While using helium as a coolant may be considered as a more innovative and promising option than water, on the other hand, the latter can rely on a widely developed and adopted technology behind. Indeed, the great majority of both conventional and nuclear power plants relies on water-based thermodynamic cycles to generate electricity. Nevertheless, the adoption of water as a coolant for the BBs shows some relevant drawbacks, having a strong impact on the tritium breeding performance as well as on the strength against irradiation embrittlement of the material. In particular, a major role on the overall performance of such a component is assigned to the First Wall (FW). Due to its position, the blanket FW has to: (a) cope with relevant heat loads (both surface and volumetric type), (b) keep structural integrity under significant mechanical loads (e.g. pressure, electromagnetic forces) as well as high-energy neutron bombardment, and (c) have a sufficiently low impact onto the tritium breeding performances of the blanket.

In this paper, a rational methodology to design and optimize the FW of a water-cooled breeding blanket is presented, taking into account an alternative design option of the Water-Cooled Lithium Lead (WCLL) BB concept foreseen for the European DEMO. In particular, the attention has been focused on optimizing the layout of the internal cooling channels, trying to increase the tritium breeding performances while complying with several thermal and structural requirements.

The outline of the paper is described in the following.

Section 2 reports briefly the architecture of the WCLL BB design option selected for the optimization, together with the main design requirements of the DEMO water-cooled breeding blanket concepts.

Section 3 reports the set-up of the multiphysics optimization problem for the improvement of the FW channels layout. In particular, the derivative-free optimization method called *Complex method* [2] is introduced, as well as the potential tritium production performance-based objective function of the WCLL BB derived by means of a heuristic

* Corresponding author.
E-mail address: ruggero.forte@unipa.it (R. Forte).

https://doi.org/10.1016/j.nme.2021.101058
Received 17 May 2021; Received in revised form 22 July 2021; Accepted 6 August 2021
Available online 25 August 2021

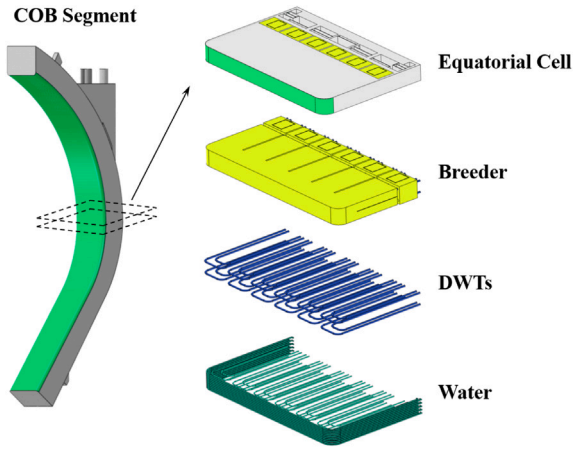

Fig. 1. Alternative design option of the WCLL Central Outboard Blanket segment.

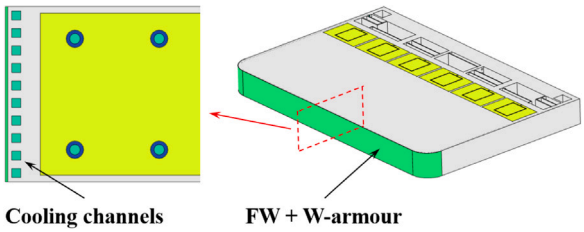

Fig. 2. Detailed view of the FW cooling channels design.

approach and verified by proper neutron transport simulations. Moreover, the thermal and structural requirements of the blanket are highlighted together with the parametric Finite Element (FE) model of the WCLL BB equatorial cell used to evaluate its thermo-mechanical response.

Section 4 reports the results of the optimization campaign, obtained by the link between the MATLAB [3] environment, where the optimization algorithm has been implemented, and the multiphysic FE model developed in COMSOL [4], that has allowed to minimize the objective function while driving the FW design towards an optimum point compliant with the imposed thermo-structural constraints.

Finally, Section 5 concerns the final assessment of the WCLL BB equipped with the optimized FW, where the results of a dedicated neutron transport analysis and detailed thermo-structural analyses are reported.

2. WCLL BB concept: Alternative design proposed for European DEMO

Blanket architecture. The WCLL BB is one of the two breeding blanket concepts currently under investigation to become the *driver* blanket for the European DEMO reactor.

Regarding the architecture of the European DEMO Breeding Blanket, it is sub-divided in sixteen toroidal sectors, each one composed of five single module segments: two inboard segments and three outboard segments. Taking the Central Outboard Blanket (COB) segment as reference, it can be thought as composed of a poloidal stack of *elementary cells*, each one identified by two consecutive toroidal–radial Stiffening Plates (SPs), as shown in Fig. 1. The structural material for all the components is Eurofer97 [5], a Reduced-Activation Ferritic/Martensitic (RAFM) steel developed during last decades by the European fusion research community.

Instead of referring to the current *reference* version of the WCLL BB (whose detailed description can be found in [6–8]), the work presented here relies on the alternative design option for the WCLL BB conceived at the University of Palermo, also in collaboration with ENEA [9,10]. While using the same design for most of the structure, the alternative concept foresees a different layout of Double-Walled Tubes (DWTs) inside the Breeding Zone (BZ), with a consequently adjustment of the manifold rear part.

The structure of the *equatorial* cell is based on a steel structure named Segment Box (SB), composed of a 25 mm-thick FW (plus 2 mm-thick tungsten-armour), two Side Walls (SWs) and a back plate, reinforced internally by a set of stiffening plates, that houses the BZ containing the breeder (Pb–17Li eutectic alloy) and the DWTs. On the rear part, a manifold region (for either water and breeder) and a Back-Supporting Structure (BSS) are placed.

As to the system of FW and SWs, Fig. 2 shows the system of internal square (7 × 7 [mm]) cooling channels, where water counter-current flow occurs, whose poloidal pitch can vary along the development of the segment depending upon the heat load distribution. Generally, the number of channel per elementary cell can vary from 4 to 10 [11].

Design requirements. The final design of the DEMO WCLL BB concept must be compliant with specific, demanding requirements related to nuclear, thermal-hydraulic and structural aspects.

The main requirement of a breeding blanket from the nuclear point of view is definitely the achievement tritium self-sufficiency by a suitable margin. The parameter onto which focus the attention is thus the Tritium Breeding Ratio (TBR), defined as the tritium nuclei produced in the blanket per D-T fusion reaction, that must be greater than 1.0. In case of a water-cooled blanket such as the DEMO WCLL BB, the tritium breeding performances can be strongly affected by the water amount used to cool down the structure, especially in the region close to plasma. This is mainly due to both its simultaneous moderation and absorption effects onto the neutrons coming from plasma.

As reported in [12], the evaluation of the tritium breeding performances in DEMO reactor is based on Monte Carlo techniques for neutron transport calculation. Of course, this approach is affected by lots of uncertainties that must be taken into account in order to exceed the minimum TBR by a *safety* margin.

The goal for the specification of a minimum design target value is to ensure a TBR ≥ 1.0 for DEMO, independently from the considered blanket concept and effects which are not taken into account in the TBR calculation, such as uncertainties of the nuclear data, blanket openings, lithium burn-up and tritium losses in the fuel cycle. Based on this rationale, the TBR design target value for the European DEMO has been set to 1.15, to be obtained by 3D Monte Carlo-based neutron transport calculations under proper modelling assumptions.

From the thermal-hydraulic point of view, several aspects need to be considered during the conception of the WCLL BB concept.

The cooling water works under PWR conditions, i.e. 15.5 MPa as operating pressure and 295–328 °C as inlet–outlet temperatures. While flowing within the blanket, the main aim is to cool down the structural components extracting the heat power deposited inside coming from the plasma.

Inside both the FW–SWs cooling channels and the DWTs, the water velocity must stay within specific limits: an upper limit of 7 m/s is due to erosion effects [6], whereas the lower limit depends basically on Departure from Nucleate Boiling (DNB) issue.

Looking at the structural requirements, several aspects have to be considered, mainly due to the extreme environment under which the DEMO BB will operate. As common in RAFM steels, Eurofer97 is characterized by good high-temperature mechanical properties (e.g. strength, ductility, creep, toughness, etc.) as well as a sufficient resistance to fast-neutron irradiation damage. However, other issues have been recognized in the application of this structural material, such as the degradation of the mechanical properties beyond a temperature of

about 550 °C, corrosion effects under lithium-lead environment and the irradiation embrittlement at low temperature.

The structure of the WCLL BB concept must be designed, hence, to work under an average temperature greater than 350 °C in the region close to the plasma, so to avoid unsustainable positive shifts of the DBTT, and, at the same time, with a maximum temperature below the upper limit of 550 °C due to properties degradation. On the other hand, such high temperatures might entail to deal with potential large creep deformations as well as relevant thermal stresses, which may involve dangerous failure modes such as plastic flow localization, exhaustion of ductility and ratcheting.

According to that, the design of the WCLL BB concept have to be developed considering all the different loading scenarios it might undergo and its structural integrity must be assessed by means of specific (nuclear) codes and standards. As far as DEMO blanket design is concerned, the EUROfusion project has selected the French nuclear standards RCC-MRx [13] as reference.

3. Multiphysics optimization

Modern, complex engineering problems such as fusion energy devices require a multiphysics approach, usually described by non-linear governing equations and subjected to multiple constraints. Optimizing them require objective functions that might be non-smooth, or time-consuming to evaluate, or in some way noisy, so that methods that rely on derivatives or approximate them via finite differences are inconvenient. According to that, the most suitable optimization algorithms might be the ones based on gradient-free approach and able to deal with multiple constraints, either physical or functional.

As stated above, the main goal of this work is to present an optimization procedure to enhance the water-cooled breeding blankets design, taking as reference the European DEMO WCLL BB concept. According to that, the optimization analysis here-presented focused on the identification of a layout for the FW cooling channels that might improve the tritium breeding performances (i.e. the TBR) of such concept, while complying with most of the severe thermal-hydraulic and structural requirements.

The goal has been achieved by means of a specific procedure, relying on a derivative-free optimization method for constrained problems developed by Box [2] and named *Complex method*, which has been properly coded into MATLAB environment. The verification of the thermo-mechanical performances of the blanket (i.e. constraints in the optimization problem) has been performed by a specific parametric FE model of the DEMO WCLL BB concept described above. A schematic view of the flow diagram representing the above-mentioned procedure is shown in Fig. 3.

The following paragraphs show details on: the version of the Complex method implemented for the optimization problem; the parametric FE model of the WCLL BB; the objective function; the constraints.

Complex method. Generally, the basic principles of an optimization problem rely on the definition of an objective function $f(\mathbf{X})$ to be minimized (or maximized), where $\mathbf{X} = \{x_1, x_2, \dots, x_n\}$ is the so-called *design vector*, containing the n design variables. If the problem is constrained, the optimization problem is subjected to both *functional* constraints and *side* constraints.

Among the several gradient-free optimization methods available, the Complex method can be considered as an extended version of the derivative-free Nelder–Mead method (also called as *Simplex method*) [14], that can be used for constrained minimization/maximization problems. It relies on the use of a geometric entity called *complex*, formed by a set of $k \geq n+1$ points in an n-dimensional space where n is the number of design variables. According to the studies carried out by Box [2], the best performance is obtained setting $k = 2n$.

The leading idea in the Complex method is to compare the values of the objective function at the k vertices of a general complex and move it gradually towards the optimum point (i.e. a minimum of the objective function) during an iterative process. The movement of the complex is achieved by using an operation known as *reflection*. As mentioned above, the Complex method can be use to both maximization and minimization process. Since the optimization activity presented in this work is based on the minimization of an objective function, only its version to be adopted in case of minimization is described in the following. The iterative procedure to be pursued in order to reach the minimum of the objective function can be summarized by the following steps:

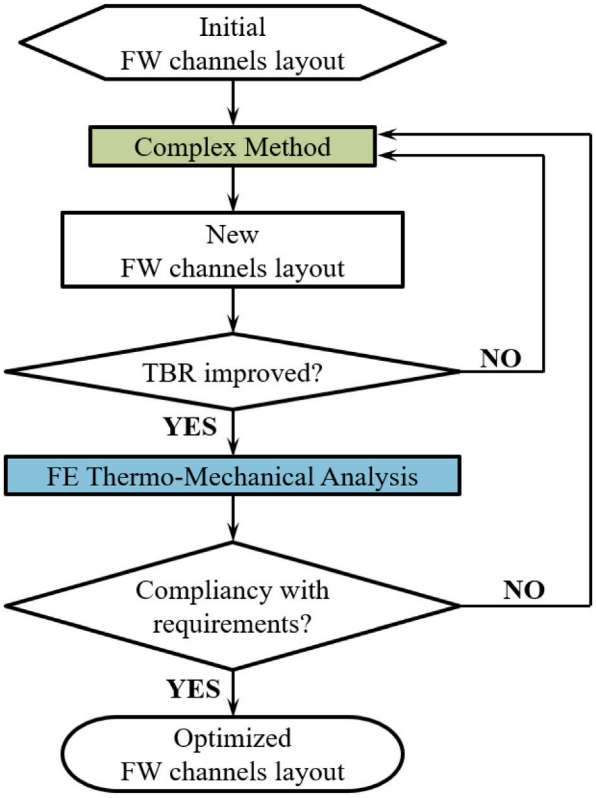

Fig. 3. Flow diagram of the optimization process.

1. Find $k \geq n+1$ points, each satisfying all m constraints. Practically, it starts with only one feasible point $\mathbf{X}_1$, and the remaining $k-1$ points are found one at a time by the use of random numbers generated in the range 0 to 1, as

$$x_i^j = x_i^{(l)} + r(x_i^{(u)} - x_i^{(l)}) \qquad i = 1, 2, \dots, n \qquad j = 2, 3, \dots, k \tag{1}$$

where x_i^j is the ith component of the point $\mathbf{X}_j$, $x_i^{(l)}$ is the lower limit of the ith design variable, $x_i^{(u)}$ is the upper limit of the ith design variable and r is a random number lying in the interval (0,1). If $\mathbf{X}_j$ violates any of the constraints, the trial point $\mathbf{X}_j$ is moved halfway towards the centroid of the remaining, already accepted points (where the given initial point $\mathbf{X}_1$ is included). The centroid $\mathbf{X}_0$ of the already accepted points is given by

$$\mathbf{X}_0 = \frac{1}{j-1} \sum_{l=1}^{j-1} \mathbf{X}_l \tag{2}$$

If the trial point $\mathbf{X}_j$ so found still violates some of the constraints, the process of moving halfway in towards the centroid $\mathbf{X}_0$ is continued until a feasible point $\mathbf{X}_j$ is found. By proceeding in this way, we will ultimately be able to find the required feasible points $\mathbf{X}_2, \mathbf{X}_2, \dots, \mathbf{X}_k$.

2. Once the initial complex is built up, the objective function is evaluated at each of the k points (i.e. vertices of the complex). If the vertex $\mathbf{X}_h$ corresponds to the highest function value, the process of *reflection* is used to find a new point $\mathbf{X}_r$ as

$$\mathbf{X}_r = (1+\alpha)\mathbf{X}_0 - \alpha\mathbf{X}_h \tag{3}$$

where $\alpha \geq 1$ (Box suggested $\alpha = 1.3$ [2]) and $\mathbf{X}_0$ is the centroid of all vertices except $\mathbf{X}_h$

$$\mathbf{X}_0 = \frac{1}{k-1}\sum_{\substack{l=1 \\ l\neq h}}^{k} \mathbf{X}_l \tag{4}$$

3. Since the problem is a constrained one, the point $\mathbf{X}_r$ has to be tested for feasibility. If the point $\mathbf{X}_r$ is feasible and $f(\mathbf{X}_r) < f(\mathbf{X}_h)$, the point $\mathbf{X}_h$ is replaced by $\mathbf{X}_r$, and we go to step 2.
If $f(\mathbf{X}_r) \geq f(\mathbf{X}_h)$, the first version of the algorithm foresaw the new trial point $\mathbf{X}_r^{(new)}$ to be obtained moving the old one halfway towards the centroid of all the vertices except $\mathbf{X}_h$, by the following relation

$$\mathbf{X}_r^{(new)} = \frac{1}{2}(\mathbf{X}_0 + \mathbf{X}_r) \tag{5}$$

and tested for the satisfaction of the relation $f(\mathbf{X}_r) < f(\mathbf{X}_h)$. If $f(\mathbf{X}_r) \geq f(\mathbf{X}_h)$, the procedure of finding a new point $\mathbf{X}_r$ moving it halfway towards the centroid $\mathbf{X}_r$ is repeated again.
Modified versions of the algorithm were then developed following the improvements suggested by Guin [15], who investigated the situations when the centroid of the complex is located either at a local minimum or inside an unfeasible region, and by Krus [16], who modified the algorithm avoiding the new reflected point and the minimum (maximum) point to get very close to each other and make the complex to collapse. A successful version of the method was also implemented by Andersson [17], where the use of a random value to be added to the new reflected point allowed to solve the above-mentioned issues. Moreover, although randomness requires some extra effort in searching for a better point in the neighbourhood of the minimum (maximum) value, it also helps to reduce the probability to get the complex stuck in a local minimum rather than the global minimum of the objective function. According to [17], in case of minimization problem Eq. (5) is replaced by

$$\mathbf{X}_r^{(new)} = \frac{\left[\mathbf{X}_r^{(old)} + \epsilon\mathbf{X}_0 + (1-\epsilon)\mathbf{X}_l\right]}{2} + (\mathbf{X}_0 - \mathbf{X}_l)(1-\epsilon)(2r-1) \tag{6}$$

where

$$\epsilon = \left(\frac{n_r}{n_r + k_r - 1}\right)^{\frac{n_r+k_r-1}{n_r}}$$

$\mathbf{X}_l$ is the point with the lowest objective function value, k_r is the number of times the reflected point has repeated itself as the one with higher objective function value with respect to the worst point $\mathbf{X}_h$, n_r is a constant (Andersson suggested $n_r = 4$ [17]). This procedure is repeated until a new point that satisfies the relation $f(\mathbf{X}_r) < f(\mathbf{X}_h)$ is found.
If an improved point $\mathbf{X}_r$, with $f(\mathbf{X}_r) < f(\mathbf{X}_h)$, cannot be obtained after a prescribed number of steps, the point $\mathbf{X}_r$ is discarded and the entire procedure of reflection is restarted by using the point $\mathbf{X}_p$, which has the second-highest function value instead of $\mathbf{X}_h$.
4. If at any stage, the reflected point $\mathbf{X}_r$ (found in Step 3) violates any of the constraints, Eq. (6) is applied until it becomes feasible.
5. Each time the worst point $\mathbf{X}_h$ of the current complex is replaced by a new point, the complex gets modified and we have to test for the convergence of the process. In particular, the convergence is obtained when the standard deviation of the function value among the complex points becomes sufficiently small, that is

$$\left(\frac{1}{k}\sum_{j=1}^{k}[f(\mathbf{X}_0) - f(\mathbf{X}_j)]^2\right)^{1/2} < \varepsilon \tag{7}$$

where $\mathbf{X}_0$ is the centroid of all the k vertices of the current complex, and ε is a specified small number greater than 0.

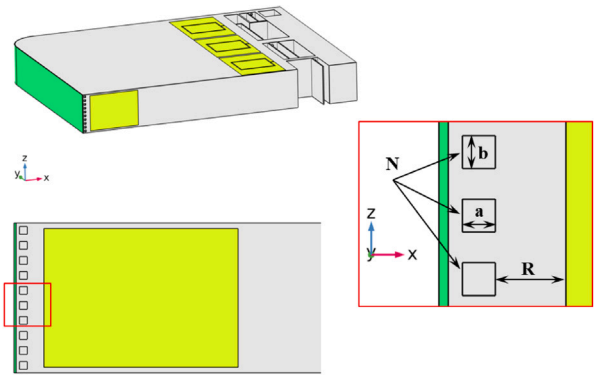

Fig. 4. Geometrical parameters of the FW cooling channels layout.

The method just described will move and modify the complex towards the minimum (maximum) of the function until all the points of the complex are featured by very similar values of the objective function, i.e. the complex is going to collapse into its centroid in proximity of the optimum point.

The Complex method has been applied to a wide range of problem areas such as fluid power system design [17], physics [18], structural engineering [19], etc. Although it was originally developed for problems with continuous variables, Haque [19] has shown that the Complex method could also be applied to mixed continuous and discrete variable problems.

WCLL BB parametric FE model. The numerical model relies on the equatorial cell of the WCLL COB segment. In particular, the model considers the structural domains (i.e. W-armour, SB, DWTs) and the breeder (see Fig. 4). In order to reduce a lot the huge computational time usually required for optimization studies, the water domain has not been modelled, but its cooling effect has been replaced by means of specific convective boundary conditions that will be described in the following sections. Moreover, exploiting its toroidal symmetry, only half model of the elementary cell has been simulated.

Since the optimization study aimed at identifying the best topology and position of the FW cooling channels layout, the geometrical model has been parametrized depending upon the definition of a certain number of design parameters related to the cooling channels layout. In particular, the uniqueness of the channels layout can be defined by means of four geometrical parameters (see Fig. 4):

- **N** [–], which is the number of channels per cell;
- **R** [mm], which represents the radial (x-axis) distance between the BZ-side of the cooling channels and the BZ itself;
- **a** [mm], which is the radial (x-axis) dimension of the cooling channel;
- **b** [mm], which represents the poloidal (z-axis) dimension of the cooling channel.

Because of the parametrization, both the geometrical and the related FE model are updated in every step of the optimization study, according the values of the parameters at that step. The full thermo-mechanical assessment of the breeding blanket requires the knowledge of the thermal field arising within the structure under the effect of heat loads and boundary conditions. Since material properties can vary a lot

with temperature, temperature-dependent thermo-physical properties of the material have been assigned to each domain. For Eurofer97, data have been drawn mainly from the RCC-MRx [13] and, when missing, from the EUROfusion material handbook [20]. As to the tungsten, the analyses have been carried out considering the data presented in [21]. Finally, the Lithium-Lead properties have been drawn from [22].

However, it must be pointed out that only Eurofer97 structural domain has been considered for the structural analyses, excluding the W-armour, being it foreseen as composed of a set of non-continuous *tiles* that should not act any significant compressive/tensile action onto the FW. As to the latter, thermo-mechanical analyses presented in [23] have shown that, if modelled as continuum solid, the presence of the W-armour adds an unrealistic compressive effect onto the FW structure, mainly due to the difference in terms of thermal expansion coefficient.

As already done in the past [9,24], two relevant operating scenarios need to be investigated for the WCLL BB design: (1) the Normal Operation (NO) scenario, and (2) the Over-Pressurization (OP) scenario.

While the former can be represented by the steady-state condition reached during the flat top of each DEMO pulse, the latter corresponds to an accidental scenario following a rupture of one (or more) DWT inside the BZ (e.g. in-box LOCA) leading to an over-pressurization of the SB.

According to that, different sets of thermal and mechanical loads and boundary conditions have to be applied during the simulation in order to investigate both the loading scenarios.

As to the thermal loads and boundary conditions, it is possible to assume preliminary that the temperature distributions in either fluids and structure do not change significantly from the NO scenario to the OP scenario (considering the first time instants after the DWT break). Hence, for the heat transfer simulation the following set of loads and boundary conditions have been used:

- surface heat flux q'' [MW/m^2] onto the W-armour plasma facing surface;
- volumetric density of nuclear-deposited heat power (or nuclear heating) q''' [MW/m^3];
- forced convective heat transfer at coolant/wall interface;
- pure diffusive heat transfer within the breeder (assumed as stagnant).

Regarding the heat flux acting onto the W-armour plasma facing surface, the value of 0.32 MW/m^2 has been applied, pertinent to the equatorial region of the COB segment [6]. The value has been applied uniformly on the straight part of the FW, whereas a cosine law has been used in correspondence of the bends connecting the FW to the SWs. The non-uniform nuclear heating distribution inside the equatorial cell has been considered by using radial profiles computed at University of Palermo by means of MCNP neutron–photon transport analyses carried out on fully heterogeneous model of a recent, similar version of the equatorial cell [25].

Although the change of the FW channels layout has an impact on the nuclear heating, this effect has been considered negligible and, hence, configuration-independent distributions have been adopted during the optimization process. Indeed, the weak dependency of the nuclear heating profiles from the cooling channels layout has been already confirmed in [26]. On the other hand, performing a neutron–photon transport simulation for each configuration would have a required a massive computational and time effort.

Since water domain is not modelled, proper convective boundary conditions have been imposed at the coolant/wall interfaces. In particular, the following iterative procedure has been adopted for each FW cooling channels layout analysed:

1. First analysis run with uniform bulk temperature set to the average temperature of 311.5 °C and initial heat transfer coefficients (different for FW channels and DWTs) computed by the Dittus&Bölter correlation [27], assuming first attempt mass flow rate for either the DWTs circuit and the FW cooling system, and calculating the coolant thermo-physical properties at its average temperature.
2. Evaluation of the power extracted by the coolant flowing through each cooling circuit (FW and DWTs) and calculation of the pertaining revised mass flow rates assuming the nominal in–out ΔT of 33 °C (295 °C–328 °C) for the coolant, as follow
$$\dot{m}_j = \frac{2\int_{A_j} q''(A_j)dA_j + Q_{nh,j}}{c_{p,ave}\Delta T} \tag{8}$$
where j stands for jth cooling circuit (i.e. FW or DWTs), A_j is the coolant-wetted surface of the jth circuit, $q''(A_j)$ is the outward heat flux crossing that surface, $Q_{nh,j}$ is the total heat power due to nuclear heating inside the water domain of the jth circuit, computed by the nuclear analysis in [25] (i.e. $Q_{nh,FWwater}$ = 10.224 kW, $Q_{nh,DWTswater}$ = 6.659 kW). The factor 2 multiplying the surface integral of the heat flux is due to the fact that thanks to its toroidal symmetry, only half of the cell has been modelled.
3. Sub-sequential analysis run with the revised heat transfer coefficients based on the mass flow rates computed in the Step 2.

By means of this iterative procedure (usually, no more than two iterations are needed), it has been possible to get more realistic heat transfer coefficients for each blanket configuration, as a function of the required mass flow rates to have the prescribed ΔT. Conversely, a first-kind boundary condition (i.e. fixed temperature) has been imposed to the water-wetted surfaces of the manifold region, considering the average temperature of 311.5 °C.

Finally, the breeder domain has been modelled as a solid domain (i.e. stagnant breeder), neglecting the contribution due to advection on its heat transport mode. This assumptions has been already adopted in several studies [28,29] and can be justified by its very low velocity inside the cell as well as the MHD effects on its flow.

As far as the mechanical simulations are concerned, the loads and the boundary conditions pertinent to both NO and OP loading scenarios have been taken into account:

- pressure loads onto the cooling water-wetted surfaces: 15.5 MPa under NO scenario and 18.6 MPa under OP scenario;
- pressure loads onto the breeder-wetted surfaces: 0.5 MPa under NO scenario and 18.6 MPa under OP scenario;
- thermal expansion induced by the thermal field predicted by the steady state thermal analysis;
- a proper set of mechanical constraints, with the aim of simulating the structural behaviour of the DEMO breeding blanket as realistic as possible (see Fig. 5).

In particular, the adopted mechanical constraints prevent the radial (x) displacement of the nodes on the back surface of the BSS and the toroidal (y) displacement of the nodes on the middle toroidal plane of

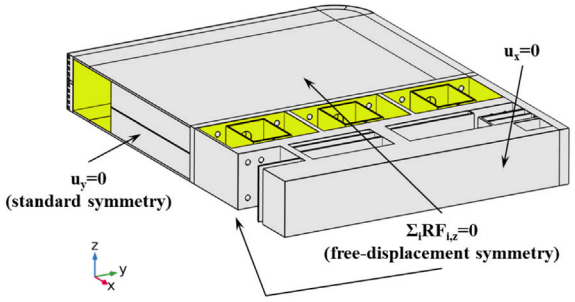

Fig. 5. Mechanical constraints on the parametric FE model of the WCLL COB equatorial cell.

the whole elementary cell. Regarding the poloidal displacement, a *free-displacement* symmetry condition has been applied to both the poloidal surfaces of the cell, in order to allow all the i nodes belonging to each symmetry plane to translate in the normal (z) direction of a uniform displacement, determined by the criterion that there is no resulting reaction force (RF) in the normal direction. Such mechanical restraints on the two poloidal surfaces based on the *plane strain* assumption have been already used in the past [24,28] and, even though it might be slightly misleading on the FW behaviour, it represents the easiest and most widely adopted option so far.

Once identified all the loads and boundary conditions acting onto the WCLL BB equatorial cell, the overall thermo-structural response of each FW channels configuration has been obtained by means of the following sequence of simulations:

1. a first study to evaluate the thermal field arising within the structure at the end of the flat top of each DEMO pulse. To do that, the above-mentioned iterative procedure has been applied and a couple of steady-state thermal analyses are carried out to converge to a final temperature distribution.
2. Two linear elastic structural analyses are performed applying only primary loads (i.e. pressure loads) pertinent to NO and OP scenario, respectively, in order to compute the primary stresses arising within the structure.
3. Finally, a linear elastic structural analysis is carried out considering only secondary loads (i.e. only thermal expansion) relying on the thermal field obtained from Step 1. From this analysis, the distribution of secondary stresses is computed.

The evaluation of the peak stresses (requiring the combined action of primary and secondary loads) has not been considered for the FW optimization analysis, and will be performed only during the final structural analysis of the optimized configuration, where it has been possible to adopt a more detailed model discretization.

Objective function. Any optimization method requires the definition of an objective function to be minimized (or maximized) to get the desired result.

Focusing on the main object of this work, the ideal objective function is represented by the hypothetical function

$$TBR(\mathbf{X}) = TBR(N, R, a, b) \tag{9}$$

where $\mathbf{X}$ is the design vector containing the four design variables identified above ($\mathbf{X} = [N, R, a, b]$).

However, the definition of a function like that above would be very demanding and tough to achieve. In fact, it would require several hundreds of neutron transport analyses and, finally, a trial of a multiple regression analysis in order to fit all the variables into a single function. Moreover, handling different kind of variables, being N a discrete variable whereas R, a and b are continuous, would make this last step much more complex. Considering the aim of this work, mostly oriented towards the definition of a general procedure, such activity has been considered out of scope, and a rational-heuristic approach has been adopted instead, identifying a potential objective function based on rational assumptions requiring less nuclear analyses.

According to that, the leading idea was to determine a scalar function $f(\mathbf{X})$ of the vectorial variable $\mathbf{X}$ so that minimizing $f(\mathbf{X})$ implies maximizing the TBR. The function $f(\mathbf{X})$ is defined as

$$f(\mathbf{X}) : \Omega \rightarrow \mathbb{R} \qquad \text{with} \qquad \mathbf{X} = [N, R, a, b] \tag{10}$$

where Ω represents the phase space of the four variables N, R, a and b.

The relation between the TBR and $f(\mathbf{X})$ has been investigated by means of several neutron transport analyses carried out on the same layout as the parametric model FE model of the WCLL BB, but considering the whole elementary cell rather than half. In particular, a numerical approach based on the Monte Carlo method has been used

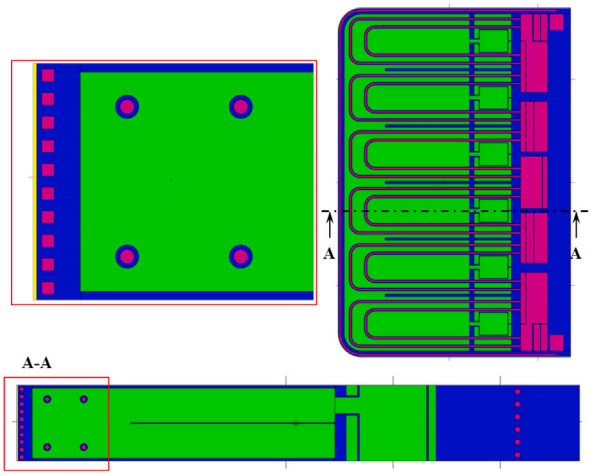

Fig. 6. 3D fully heterogeneous, parametric MCNP model of the WCLL COB equatorial cell (configuration with N = 10, R = 15 mm, a = 7 mm, b = 7 mm).

Table 1
Matrix of cases with TBR results.

Case	N [–]	R [mm]	**a** [mm]	**b** [mm]	TBR [–]
#1	10	15	7	7	3.207E–01
#2	5	15	7	7	3.141E–01
#3	10	5	7	7	3.313E–01
#4	5	5	7	7	3.191E–01
#5	10	9.75	12.25	4	3.216E–01
#6	10	18	4	12.25	3.189E–01
#7	5	9.75	12.25	4	3.153E–01
#8	5	18	4	12.25	3.134E–01
#9	10	8	14	7	3.395E–01
#10	5	6.75	15	5.4	3.222E–01
#11	5	13	7	7	3.149E–01
#12	5	5.3	13.8	20.8	3.621E–01

adopting the MCNP5.1.6 code [30] along with the JEFF3.2 cross section libraries [31]. A fully heterogeneous, parametric 3D MCNP model of the equatorial slice has been set up (see Fig. 6), and the planar neutron source built-up within a recent collaboration between the University of Palermo and the Karlsruhe Institute of Technology [32,33] has been used.

In particular, such source takes into account both the neutrons coming directly from the plasma (D-T reactions) and the neutrons due the albedo in the whole DEMO reactor. It has been developed handling the results obtained adopting a MCNP model of the whole reactor with its proper neutron source simulating a D-T plasma. More precisely, both the neutrons and photons crossing the plasma facing surface of the selected slice have been sampled in energy and cosine bins to be able to set up a proper source for the slice MCNP input in a similar way as done in [32] and [33]. As far as the boundary conditions are concerned, pure reflecting boundary conditions have been imposed to the top and bottom poloidal surfaces, whereas *white* boundary conditions [34] have been applied to the toroidal direction, as already used in [33] and discussed in depth in [35].

With the aim to investigate how the tritium breeding performance of the elementary cell is affected by the water amount and distribution in the FW, eight MCNP models have initially been analysed (Case #1 to Case #8 in Table 1), each one equipped with a different FW channels layout. The analyses have been carried out by simulating a large number of histories ($\sim 10^{10}$) so that the results obtained are affected by relative errors lower than 1% even in the slice regions more distant from the source.

As shown in the table, the first investigation carried out was to assess the impact of the water amount (represented by the term $N \cdot a \cdot b$), without changing neither the aspect ratio of the channel (i.e. b/a) nor

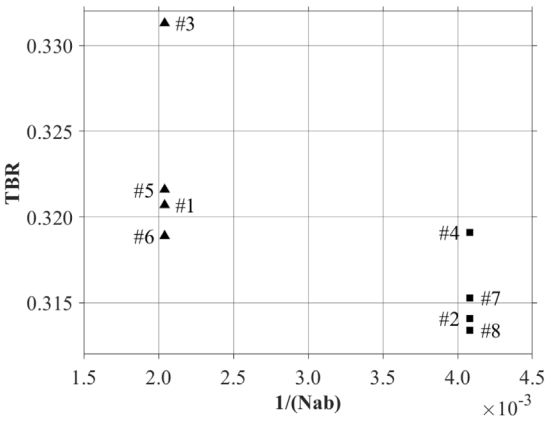

Fig. 7. TBR vs. $1/Nab$.

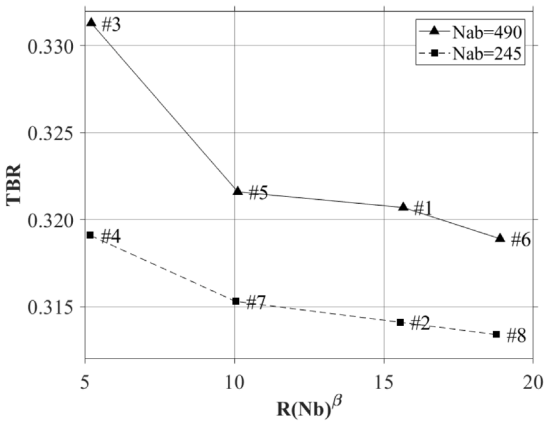

Fig. 8. TBR vs. $R(Nb)^{\beta}$ with $\beta = 0.01$.

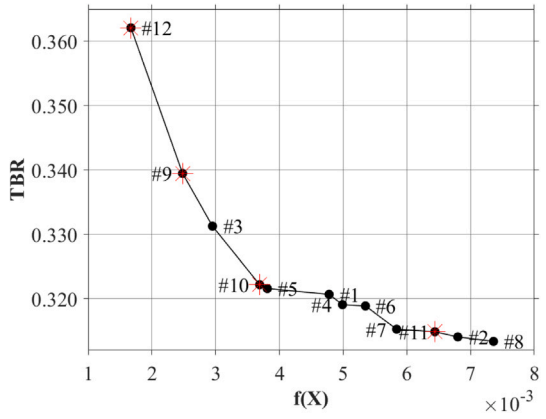

Fig. 9. TBR vs. $f(\mathbf{X})$.

the distance R. In order to do that, two cases equipped with 10 and 5 cooling channels (Case #1 and Case #2, respectively) have been analysed, considering the reference dimensions of the channels (7 mm × 7 mm) with $R = 15$ mm.

Secondly, starting from the first two cases, the impact of the distance between the channels and the BZ has been evaluated reducing R from 15 mm to 5 mm, for both the configurations with 10 (Case #3) and 5 (Case #4) cooling channels.

Finally, other four simulations (from Case #5 to Case #8) have been performed keeping, for the two main cases #1 and #2, the same number of channels N as well as the water amount Nab but changing the aspect ratio b/a of the channels, together with R accordingly. For each configuration the channels have been re-arranged and equally spaced along the poloidal direction.

In order to better understand the results obtained, two different plots are reported below. In particular, Fig. 7 shows the TBR performances of all the layout analysed as a function of the reciprocal of the total cross-sectional area of the channels (i.e. $1/Nab$), which is inversely proportional to the water amount inside the FW.

Looking at the results, it is easy to observe that the water amount plays a pivotal role in the increase/decrease of the TBR and, in particular, higher is the water amount higher is the TBR. Such unexpected result goes towards the opposite direction of what observed in [11] and stated also in [12], and further investigations would be needed to get to know which are the modelling assumptions (i.e. heterogeneous vs. homogeneous model and elementary cell vs. whole blanket sector) that make such a difference come out. Such behaviour is probably due to the volumetric ratio between steel and water, so that the lower this ratio, the greater the production of tritium since the softer spectrum promotes tritium reactions to the detriment of parasitic absorptions in the structural material whose percentage content in the FW decreases.

From Fig. 7 it was also possible to observe that, for each level of water amount, a certain behaviour exists between different configurations. In particular, it was found that the TBR increases when the quantity $R(Nb)^{\beta}$ (with $\beta \in \mathbb{R}$) decreases, as shown in Fig. 8.

This last plot shows that the reduction of the parameter R has a positive influence on the tritium breeding, as already noted in [26], as well as the reduction of the poloidal surface occupied by the channels Nb, with a second-order effect though.

In fact, as already stated in [26], both contributes to the reduction of the steel thickness enclosed between the channels and the BZ, wherein lots of neutrons are captured after having been moderated by the water.

Combining both the aspects observed in Figs. 7 and 8, a unique scalar function $f(\mathbf{X})$ of the design variable vector $\mathbf{X}$ has been defined by a linear combination between $1/Nab$ and $R(Nb)^{\beta}$ as follow,

$$f(\mathbf{X}) = \frac{1}{Nab} + \gamma R(Nb)^{\beta} \tag{11}$$

where $\beta = 0.01$ and $\gamma = 1.75 \cdot 10^{-4}$. In particular, the low value of the coefficient β justifies the weak influence of the factor Nb with respect to R, whereas the coefficient γ combines the two addends of the function in terms of magnitude. Plotting the TBR obtained vs. the function $f(\mathbf{X})$ (see Fig. 9), it is possible to observe how the minimization of the latter implies an increase of the TBR.

However, being the function in Eq. (11) not bijective (i.e. different combinations of the design variable may have the same value of the function), it must be stressed that is not possible to assert that the TBR is function of $f(\mathbf{X})$. Indeed, two different vectors $\mathbf{X}_i$ and $\mathbf{X}_j$ might have the same value of the function $f(\mathbf{X})$, but show different values of TBR. In math formulation, it cannot be shown that

$$f(\mathbf{X}_i) = f(\mathbf{X}_j) \implies TBR(\mathbf{X}_i) = TBR(\mathbf{X}_j) \tag{12}$$

According to that, before implementing the function in Eq. (11) as the objective function to be minimized in our multiphysics optimization framework, its goodness has been also tested with other four different cases (Case #9 to Case #12 in Table 1) to verify if it is at least sufficiently monotonic in the interval of interest for the problem's purposes.

As expected, the four additional configurations analysed confirmed the trend already outlined by the first eight simulations, without showing any inversion of concavity. Furthermore, even though $f(\mathbf{X})$ is not bijective, it can be agreed that combinations of parameters having similar values of the objective function, show also similar values of TBR.

Such heuristic approach has been used to obtain, without performing hundreds of MCNP calculations, an acceptable objective function to be easily implemented in such multiphysics optimization framework in

order to increase the tritium breeding performances in the equatorial cell of the WCLL COB segment. Moreover, having been confirmed by neutron transport calculations, the function in Eq. (11) might represent a good starting point for further studies in the development of a general function $TBR(\mathbf{X})$.

Constraints. As far as the constraints are concerned, their definition had to deal with different aspects of a water-cooled breeding blanket design. In particular, as already described above, two different types of constraints had to be defined: (1) the *side constraints*, that are the limits of the design variables, and (2) the *functional constraints*, depending upon the performances and the prescribed requirements.

The design variable limits have been defined relying on the recent experiences in the WCLL BB design [6,23] as well as on rational assumptions. In particular, the following intervals have been adopted for the design variables N, R, a and b during the optimization process:

$$N \in [4\,;\,10] \subset \mathbb{N} \tag{13}$$

$$R \in \left[s\,;\,t_{FW} - 3s\right] \subset \mathbb{R} \tag{14}$$

$$a \in \left[2s\,;\,t_{FW} - R - s\right] \subset \mathbb{R} \tag{15}$$

$$b \in \left[2s\,;\,(H - Ns)/N\right] \subset \mathbb{R} \tag{16}$$

where $s = 2$ mm, assumed as the minimum thickness of any section in the FW domain, $t_{FW} = 25$ mm, that is the FW thickness, and $H = 135$ mm, that is the poloidal height of the elementary cell. Concerning the channel dimensions a and b, a lower limit of 4 mm has been imposed to both dimensions, whereas the upper limits depend on the values of the R and N, respectively.

As to the functional constraints, since the main nuclear requirement (i.e. the TBR) has been considered during the objective function definition, only thermal-hydraulic and structural requirements have been imposed for the FW optimization. In particular, considering the coarseness of the numerical model used for the optimization, not all of the requirements presented above have been implemented, but the ones identified as the most critical for our purposes.

Regarding the thermal-hydraulic constraints, limitations on coolant maximum velocity as well as on maximum or minimum temperature in the structure have been implemented:

$$u_{FW} \leq 7 \text{ m/s} \tag{17}$$

$$T_{Eurofer,max} \leq 550\ ^{\circ}\text{C} \tag{18}$$

$$T_{SLi,ave} \geq 350\ ^{\circ}\text{C} \tag{19}$$

where u_{FW} is the average coolant velocity in the FW cooling channels, $T_{Eurofer,max}$ is the maximum temperature reached in the Eurofer97 domain, and $T_{SLi,ave}$ is the average temperature on the ith Supporting Line (SL_i), defined to perform the stress linearization procedure. As to the latter, those limits have been imposed due to DBTT considerations stated in [36].

From the structural point of view, constraints on the verification of some of the RCC-MRx design criteria have been imposed. In particular, the structural performances of each FW configuration analysed have been evaluated out adopting the linear elastic approach as suggested in the RCC-MRx. Such code foresees the use of the stress linearization procedure to be performed in the most critical regions of the component. In order to do that, a set of Supporting Lines (SLs) is identified, placed along the thickness of the sections to be assessed. As far as the parametric FE model of the equatorial cell, the attention has been focused on the object of the optimization, i.e. the complex of FW and SW. In particular, a set of ten (parametric) supporting lines have been selected, as shown in Fig. 10, placing six of them at the middle of the FW, whereas other four ones in correspondence of the bend between the FW and the SW.

Such set of paths allows to check the stress level in correspondence of the most relevant sections of the FW, looking at the points with maximum bending (i.e. SL 1, SL 2, SL 3, SL 7) and maximum resulting moment (i.e. SL 9, SL 10). Furthermore, the region at the FW bend (i.e. SL 4, SL 5, SL 6, SL 8) needs also attention due to bending effects.

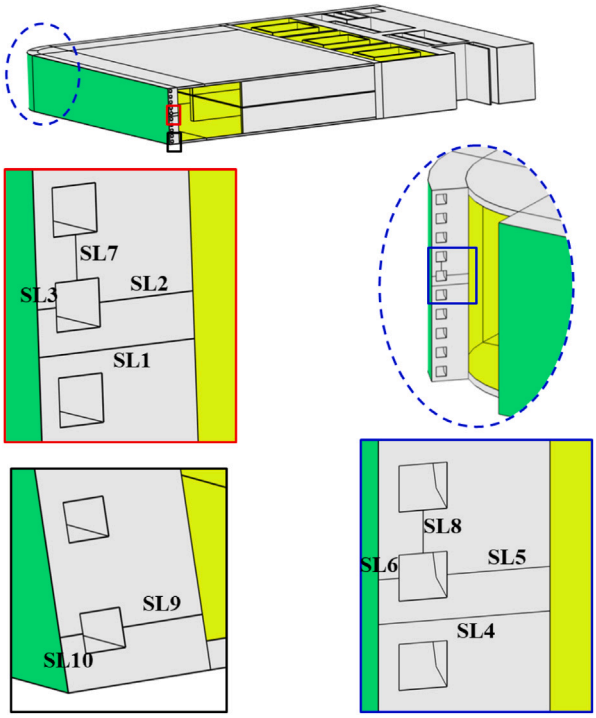

Fig. 10. Supporting lines used for stress linearization procedure.

As already described in the section concerning the structural requirements, the verification of the design criteria is performed comparing an equivalent stress, combining different kind of stresses depending upon the criterion, with the specific allowable stress presented above, depending also upon the service level. In particular, according to the standards, the NO and the OP scenarios are classified as Level A and Level D, respectively.

The following main RCC-MRx design criteria have been adopted:

$$(\overline{P_m}) \leq S_m \tag{20}$$

$$(\overline{P_L + P_b}) \leq 1.5S_m \tag{21}$$

$$(\overline{P_m + Q_m}) \leq S_{em} \tag{22}$$

$$(\Omega\overline{P_m}) \leq S_t(t) \tag{23}$$

$$(\overline{P_L + \Phi P_b}) \leq S_t(t) \tag{24}$$

$$(\max\left[\overline{P_L + P_b}\right] + \overline{\Delta Q}) \leq 3S_m \tag{25}$$

where P and Q are the primary and secondary stresses, respectively, while S refers to different allowable stresses. For a detailed description of both symbols and criteria, the reader is addressed to the standards [13]. For creep failure considerations, an activation temperature of 450 °C has been set as lower limit, mainly due to lack of data at lower temperatures, and an operating time of 18 000 h (≈2 full-power year) has been assumed for the blanket. As to the verification against ratcheting failure mode, $\overline{\Delta Q}$ has been conservatively approximated to $\overline{Q}$, having been considered only one steady-state thermal analysis.

In order to take into account uncertainties on temperature distribution, a small safety margin n (=1.05) on the allowable stresses has been considered.

4. Results of the optimization campaign

The definition of the initial complex requires that the first point must be feasible. According to that, its choice was driven by the

reference FW channels layout in the equatorial region of the COB segment [11], which is featured by $N = 6$, $R = 15$ mm, $a = 7$ mm and $b = 7$ mm.

However, the check on its feasibility resulted in the violation of several thermo-structural constraints, all of them concerning the minimum average temperature in the main thicknesses of the FW, as in Eq. (19). In particular, the average temperature in lines SL3, SL6, SL7, SL8 and SL10 (see Fig. 10) was below 350 °C. If reducing R from 15 to 14 mm was sufficient to satisfy the requirement in lines SL3, SL6 and SL10, no feasible actions were identified to make the average temperature between two consecutive channels (SL7 and SL8) higher than 350 °C.

With the aim of finding other feasible points that fulfil all the prescribed requirements, lots of configurations have been analysed but none of them was able to satisfy contextually all the constraints inherent to either stress limits and minimum irradiation temperature due to DBTT positive shifts effects.

Nevertheless, being non-productive to relax the constraint to a lower temperature [36], it has been decided to remove such temperature constraint from the thicknesses along the lines SL7 and SL8. In fact, the eventual crack nucleation and propagation along the thickness separating two water channels can be considered as less relevant than along thicknesses separating the coolant from other environments (i.e. BZ, plasma chamber). Furthermore, a temperature constraint in the thickness between channels is somehow considered in the minimum allowable average temperature along the lines SL1 and SL4.

Despite that, irradiation embrittlement in the material very close to the water cooling channels will definitely occur and, if not properly tackled, such phenomenon might cause gross failure of the FW. Hence, it is important to underline how much further R&D activities on fusion reactor materials is still needed, so to allow the designers to conceive feasible, reliable and performing components.

Once the first feasible point was identified, the initial complex has been randomly determined by means of Eq. (1).

Since the Complex method is intrinsically unable to recognize a local minimum from the global minimum of a function, good rationale to investigate more deeply the feasible n-dimensional space is to run more than a single optimization analysis and compare the final results obtained. According to that, five simulations have been carried out for the optimization of the FW cooling channels, each one starting with a different initial complex.

The procedure made of sequential reflections and shaping of the complex to reach the minimum of the objective function (while complying with the constraints) is shown in the Figs. 11 and 12. The former reports in a log–log graph the objective function value at the centroid of the complex $f(\mathbf{X}_0)$ vs. the number of reflections completed, while the latter reports in a log–log graph the standard deviation value of the complex σ as defined in Eq. (7) vs. the number of reflections completed.

In order to make both calculation and visualization easier, the objective function $f(\mathbf{X})$ has been scaled with a multiplication factor of $1 \cdot 10^3$, so to obtain values in the order of the unity. In fact, such operation does not modify the outcome of an optimization process. As a consequence of that operation, the minimum threshold ε, as defined in Eq. (7), has been set to $1 \cdot 10^{-2}$, in order to have a deviation between the objective function value at each point and the value at the centroid lower than $1 \cdot 10^{-1}$ on average.

The final results show that around 25÷65 reflections are necessary to get the standard deviation σ lower than $1 \cdot 10^{-2}$, depending upon the initial complex (see Eq. (1)) and that little of randomness acting during the optimization process (see Eq. (6)). However, similar values of the objective function have been reached at the end of the five runs, even if obtained with different combinations of variables. In particular, Run #5 is the simulation that ended up with the lowest objective function value, as shown in Fig. 11. According to the detailed results described in Appendix, the optimum point identified by the last run has got an objective function value of 1.881, featured by $N = 5$, $R = 6.194$ mm, $a = 13.744$ mm and $b = 19.497$ mm.

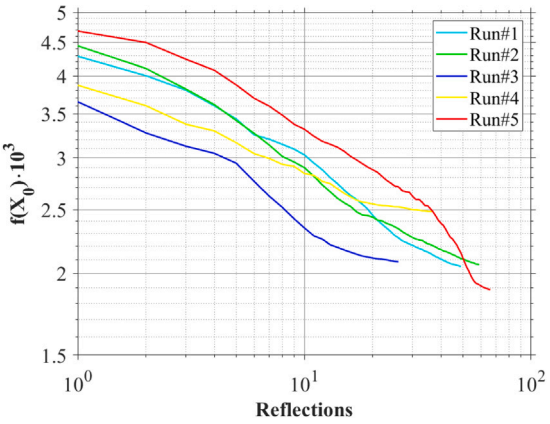

Fig. 11. Objective function value at centroid vs. number of reflections.

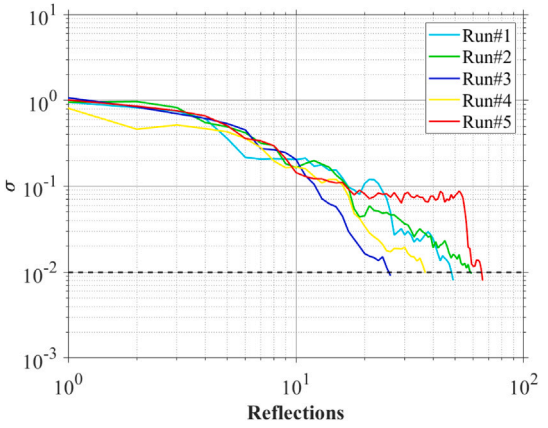

Fig. 12. Standard deviation of $f(\mathbf{X})$ vs. number of reflections.

5. Assessment of the optimized design

In this last chapter, a more detailed multiphysics assessment of the WCLL COB equatorial cell equipped with an optimized FW channels layout is reported. As obtained at the end of the optimization campaign presented in the previous chapter, the selected optimized layout of FW cooling channels is featured by $N = 5$, $R = 6.194$ mm, $a = 13.744$ mm and $b = 19.497$ mm.

Since such tolerances are not significant for manufacturing such kind of component, the dimensions in the final layout have been approximated so to give more reasonable values as follow: $N = 5$, $R = 6.2$ mm, $a = 13.7$ mm and $b = 19.5$ mm.

The first section of the chapter regards to the preliminary nuclear analysis performed to evaluate the TBR performances as well as the specific nuclear heating profiles to be adopted for the thermo-mechanical analysis.

Secondly, a more detailed thermo-mechanical analysis of the equatorial cell is carried out, evaluating its global thermal-hydraulic parameters as well as the temperature distribution in the several domains. The latter is, then, used together with pressure loads to perform the mechanical analyses and compute the primary, secondary and primary plus secondary stress distributions arising within the structural domain in both NO and OP loading scenarios.

Finally, the enhanced elastic approach as per RCC-MRx is applied to carry out the structural integrity assessment of the component, focusing the attention on the FW domain, and evaluating strengths and weaknesses of the optimized design against the most relevant failure modes for nuclear irradiated components.

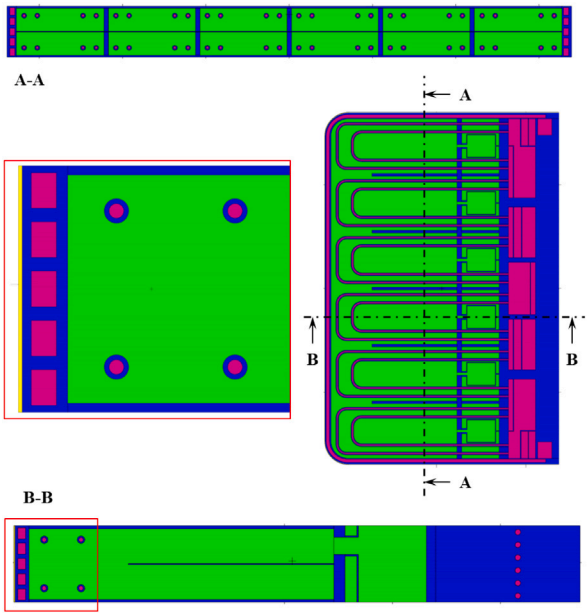

Fig. 13. 3D fully heterogeneous model of the WCLL COB equatorial cell equipped with the optimized FW.

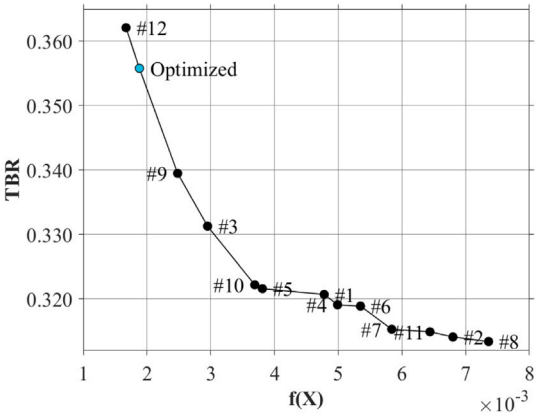

Fig. 14. TBR performances of the optimized layout.

5.1. Nuclear assessment

Following the same approach as during the definition of the objective function, the TBR performances of the optimized concept has been evaluated. A fully heterogeneous 3D MCNP model of the optimized equatorial slice has been set up (see Fig. 13), and the same planar neutron source and boundary conditions as those adopted for the definition of the objective function have been applied.

The analyses have been carried out by simulating a large number of histories ($\sim 10^{10}$) so that the results obtained are affected by relative errors lower than 1% even in the slice regions more distant from the source.

The nuclear response of the equatorial cell has been investigated focusing the attention onto the TBR performances as well as onto the neutronic and photonic deposited power. As far as the tritium breeding performances are concerned, the global evaluation of the tritium produced has been computed and equal to 0.3558. Plotting this result inside the graph of Fig. 9, it is still in good agreement with the definition of the objective function $f(\mathbf{X})$ (see Fig. 14).

The results show also a very positive increment of the TBR thanks to the optimized layout with respect to the cases #1 (+10.95%) and #2 (+13.28%), that can be considered as reference values being the number of FW channels varying from 4 to 10 poloidally along the COB segment while keeping $R = 15$ mm, $a = 7$ mm and $b = 7$ mm.

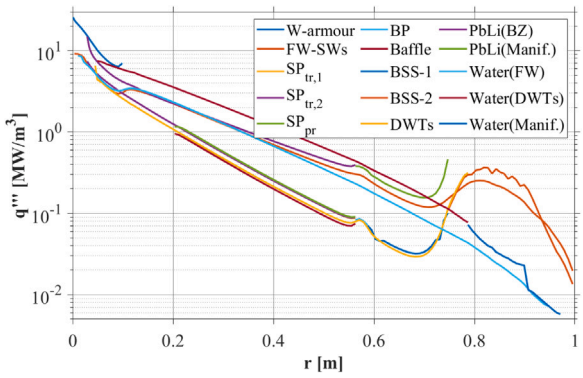

Fig. 15. Radial profiles of the deposited nuclear power volumetric density q''' in the optimized WCLL COB equatorial cell.

The spatial distribution of the deposited nuclear power volumetric density (i.e. nuclear heating), q''', was evaluated to allow the study of the thermo-mechanical performances to be carried out. In particular, its radial profiles were assessed within several sub-domains of the cell, as shown in Fig. 15.

As expected, the deposited power densities reach their highest values near the plasma-facing region of the segment, both in the SB and the BZ, decreasing significantly along the radial direction.

The highest value of around 26 MW/m^3 is reached in the W-armour, which is the layer directly facing the plasma. The average value of nuclear power deposited in the FW is around 8÷9 MW/m^3, in agreement with what calculated in [11,26]. The maximum value of q''' obtained in the breeder is around 14.9 MW/m^3. Finally, it is worth to notice the appearance of peaks and, more general, of increased values in the rear region of the cell, probably due to *back-scattering* of the neutrons in those regions induced by the significant amount of water contained in the manifold close to the BSS. However, such effect involves regions featured by nuclear power density values decreased of almost two order of magnitude with respect to the highest values.

5.2. Thermo-structural assessment

The thermo-structural assessment of the optimized configuration of the equatorial cell has been carried out adopting the same procedure as the one used for the optimization campaign, but relying on a more detailed numerical model as well as specific loads and boundary conditions.

As to the heat transfer analysis, The same kind of thermal loads and boundary conditions used for the optimization campaign have been adopted for the computation of the temperature distribution in the model. According to that, the main difference with respect to the thermal field computed during the optimization analysis is the nuclear heating distribution inside the cell, this time calculated specifically for this geometry as shown in Fig. 15.

The maximum temperature in the Eurofer97 of 544 °C has been computed, slightly below the maximum allowable limit of the material set to 550 °C.

As far as the FW–SW system is concerned, the maximum temperature is around 435 °C in correspondence of the interface with the W-armour, whereas the minimum value is very close to the fluid bulk temperature of 311 °C.

The temperature distributions obtained in the FW domain from the steady-state heat transfer analysis is reported in Fig. 16.

With regards to the mechanical analysis of the equatorial cell equipped with the optimized FW, the same loads and the boundary

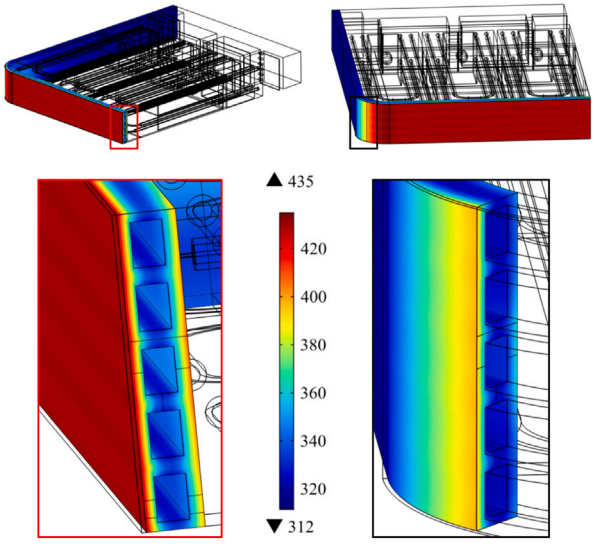

Fig. 16. Temperature [°C] distribution in the system of FW–SW.

conditions used for the optimization campaign and pertinent to both NO and OP loading scenarios have been applied.

With particular attention to the FW, the global Von Mises stress fields have been plotted in Fig. 17 for both the NO and OP scenarios.

With regards to the OP loading scenario, primary stresses become very significant due to the huge increment of the internal pressure inside the SB (0.5 MPa vs. 18.6 MPa). Such a high value of pressure load generates a relevant bending of the FW, implying high stresses concentrated in correspondence of the joint with the toroidal–radial SPs.

Nevertheless, it must be pointed out that those high stresses might be caused by the mechanical plain strain boundary conditions applied along the z-direction, which perhaps generates an excessive compressive effect on the FW. In particular, the arise of a radial decreasing temperature profile in the structure together with imposing a uniform poloidal deformation ($\epsilon_z(x, y)$ = const.) to both upper and lower surfaces of the cell, forces the hottest and the coldest regions to undergo the same poloidal deformation, putting hence the regions near the plasma under compression while the rear ones under tensile.

The structural integrity assessment of the optimized FW has been carried out relying on the numerical results obtained by means of the thermo-mechanical analyses presented above, and following the linear elastic approach outlined in the RCC-MRx.

According to what already described above, a set of supporting lines wherein perform the stress linearization has been identified in the FW–SW domain, focusing the attention on the main relevant thicknesses to be checked. With respect to the paths selected for the optimization campaign, the more detailed discretization has allowed to select two additional supporting lines (SL#11 and SL#12) located in correspondence of the junction between the FW and the toroidal–radial SPs, as shown in Fig. 18.

With regards to the design criteria without considering neither creep nor irradiation effects, failure due to plastic collapse and instability has been assessed, and the results are reported in Table 2 for both Level A and Level D in terms of ratio between the applied and the allowable stress.

The results show that, as to the normal operation, both criteria are satisfied in all the selected supporting lines, whereas failure for plastic instability occurs in paths SL11 and SL12 considering the Level D scenario (bold values in Table 2). Indeed, the over-pressurization of the SB generates a significant bending of the FW causing a high resultant moment in correspondence of the junction between the FW and the toroidal–radial SPs.

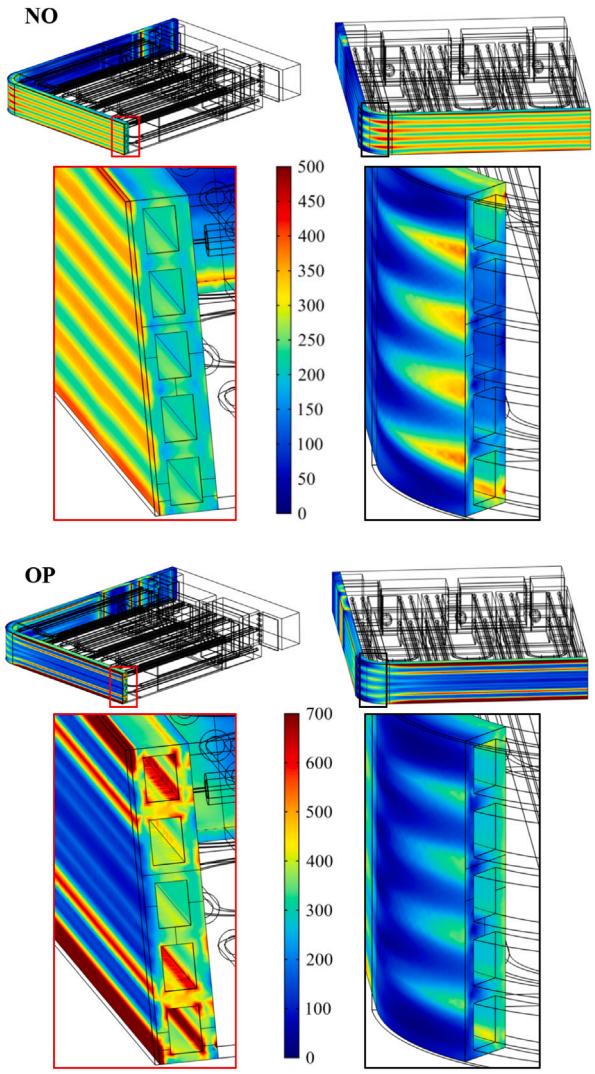

Fig. 17. Von Mises stress [MPa] distribution in the system of FW–SW under NO (top) and OP (bottom) scenario.

Table 2
Results for plastic collapse and instability. The S_m allowable stresses drawn from [13].

Path	T_{ave} [°C]	$(\overline{P_m})_A/S_{m,A}$	$(\overline{P_L+P_b})_A/1.5S_{m,A}$	$(\overline{P_m})_D/S_{m,D}$	$(\overline{P_L+P_b})_D/1.5S_{m,D}$
SL1	366.8	0.138	0.095	0.369	0.309
SL2	378.9	0.084	0.159	0.403	0.353
SL3	395.3	0.105	0.283	0.630	0.609
SL4	346.4	0.138	0.106	0.341	0.556
SL5	347.6	0.061	0.178	0.722	0.627
SL6	372.4	0.131	0.237	0.125	0.201
SL7	331.3	0.260	0.175	0.443	0.299
SL8	324.2	0.259	0.178	0.342	0.236
SL9	371.2	0.101	0.202	0.798	0.818
SL10	395.2	0.086	0.248	0.588	0.403
SL11	371.6	0.179	0.123	0.575	**1.590**
SL12	395.9	0.292	0.299	0.724	**1.446**

As to the cyclic loads when both creep and irradiation are neglected, failure against ratcheting and fatigue in non-singular zones have been verified. Since no thermo-mechanical analysis has been performed at the end of the cycle, the stress has been conservatively assumed to vary between zero and maximum of the cycle (i.e. $\Delta\sigma \approx \sigma$). The results obtained applying the $3S_m$ rule for progressive deformations have been reported in Table 3.

The results obtained show that no sections undergo failure for ratcheting, where the lowest margin has been computed in correspondence of the thickness separating the cooling channel from the W-armour.

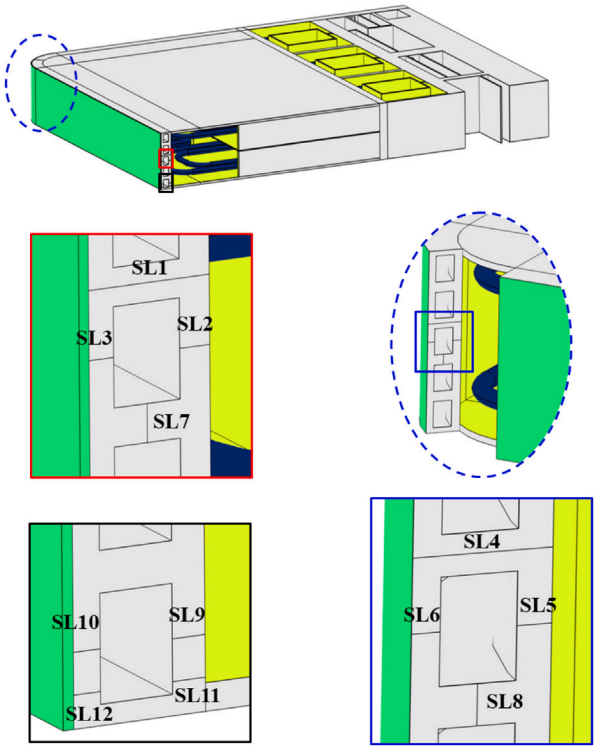

Fig. 18. Enhanced set of supporting lines used for stress linearization procedure.

Table 3
Results for ratcheting.

Path	$(\max\left[\overline{P_L+P_b}\right]+\overline{\Delta Q})_A/3S_{m,A}$
SL1	0.388
SL2	0.492
SL3	0.725
SL4	0.266
SL5	0.232
SL6	0.564
SL7	0.508
SL8	0.259
SL9	0.577
SL10	0.693
SL11	0.524
SL12	0.669

Considering the irradiation effects, low temperature rules (i.e. negligible creep) to prevent immediate plastic flow localization and immediate fracture due to exhaustion of ductility have been also checked and all criteria have been fulfilled.

As far as the damage caused by creep is concerned, the activation temperature for Eurofer97 is around 450 °C. Hence, looking at the average temperature of the selected paths in the FW domain under nominal operating conditions (see Table 2 for example), all of them are lower than 400 °C and, thus, no creep failure is predicted in the FW domain, according to the available data.

Furthermore, those temperature profiles are also helpful to identify potential region when irradiation embrittlement can occur with a major impact, causing large positive shift of the DBTT.

During the optimization campaign, a lower constraint was considered on the average temperature of the majority of selected paths in the FW domain, fixing a minimum value of 350 °C, according to [36].

The results obtained from the heat transfer analysis of the optimized FW have positively shown that the majority of the FW thicknesses are characterized by an average temperature lying in the range 350–400 °C, which is optimal to avoid either severe irradiation embrittlement and creep deformation. The paths showing an average temperature lower than 350 °C are SL4 and SL5, located in the FW corners but both very close to the limit (≈ 347 °C), together with SL7 and SL8. Although the average temperature on the latter are quite below 350 °C, crack propagation along those paths can be considered as of less importance, referring to thicknesses separating two consecutive cooling channels instead of different environments (i.e. cooling channels/breeder zone or cooling channels/plasma chamber).

In general, the structural integrity assessment carried out on the optimized FW of the equatorial cell of the WCLL COB segment shows that the structure withstand safely the normal operating conditions, considering both primary and secondary loads. Moreover, no significant creep deformation has been predicted within the FW–SW domain. On the other hand, particular attention needs to be addressed to the OP scenario, where small regions close to the junction between the FW and the toroidal–radial SPs undergo failure for plastic collapse and instability.

6. Conclusions

The main topic of such activity concerned the development of a multiphysics tool to be used for optimizing the design of the water-cooled breeding blanket concept foreseen for DEMO, taking into account its nuclear, thermal-hydraulic and thermo-mechanical design aspects. In particular, the attention has been focused on the internal cooling channels housed within the system of FW–SWs, trying to figure which is the best layout for maximizing the tritium breeding performances of the blanket without undermining its structural integrity.

In order to do that, the derivative-free Complex method has been applied for the design optimization of the European DEMO WCLL breeding blanket concept. To this purpose, a potential performances-based objective function to be minimized has been defined by means of a heuristic approach and validated by neutron transport analyses. Moreover, a parametric multiphysics FE model of a single equatorial cell of the Central Outboard Blanket segment (relying on an alternative concept developed at University of Palermo) has been developed in order to solve the coupled thermo-mechanical problem and check the fulfilment of the prescribed functional and structural requirements. Using a link with MATLAB, wherein the optimization algorithm has been implemented, the optimization campaign led the design towards an optimum point compliant with the adopted constraints.

Considering such a complex multiphysic problem as the fusion breeding blanket design, the adoption of the Complex method has allowed to successfully enhance the design of the WCLL BB, focusing on a particular component such the FW, with a much lower number of numerical analyses than the huge amount usually required by a conventional parametric sweep approach, where conversely hundreds (or even thousands) of analyses could be needed to properly investigate all the phase space of the variables and to identify an optimized configuration.

Once obtained the optimized design, its nuclear, thermal-hydraulic and structural performances have been investigated with more detailed numerical models.

From the nuclear point of view, the new layout of the FW cooling channels allows an increment in TBR performances up to around 10% and 13% with respect to the Case #1 and Case #2, respectively, that are actual potential configurations under investigation for the WCLL BB. Being always been a weakness of the water-based breeding blanket, this achievement is surely very promising. Nonetheless, it must be pointed out that the actual increment in terms of TBR presented in this work is related to the modelling assumptions here adopted. The absolute gain should be validated by proper 3D neutron transport analysis of the machine.

As far as the thermo-mechanical performances are concerned, the highest temperature reached in the Eurofer97 structure of the equatorial cell is lower than the maximum allowable limit of 550 °C. The optimized FW withstand safely the design criteria reported in the RCC-MRx concerning the Normal Operation scenario (Level A), while the

region in correspondence of the joint with the toroidal–radial SPs might undergo failure for plastic instability. No significant creep deformation has been predicted in the FW domain being the average temperature along the most relevant sections lower than 400 °C. However, it must be highlighted that some regions of the FW–SWs system might suffer irradiation embrittlement due to the low operating temperature of the coolant. Indeed, the material close to the cooling channels will undergo high dpa damage working with an operative temperature lower than 350 °C, causing thus a positive shift of the DBTT quite above the room temperature. This latter aspect might introduce several problems involving the start-up and shut-down scenarios of the components, as well as its maintenance and the removal, that have to be properly managed relying for instance on thermal annealing and/or pre-heating procedures. Nevertheless, the approach followed in this work is based on the verification of structural design rules relying on linear analysis results. Due to the strong nonlinear behaviour of both creep deformation and loss of ductility, more dedicated nonlinear analyses are encouraged to investigate deeply the arising of such phenomena in the material and, hopefully, relax some stringent thermo-mechanical requirements.

The overall activity shows that some improvements in water-cooled breeding blankets can be achieved decreasing the volumetric ratio between steel and water in the FW to enhance the moderating effect of the latter in favour of Tritium breeding reactions in the BZ rather than neutron absorptions in the structural material. On the other hand, more R&D activity on the structural materials to be used in the blanket is still needed if we want to enhance the design of such a component. Both high irradiation and high temperature cause severe strain to the material and, in order to get sustainable lifetime for the future fusion reactors, its performances under such extreme environments have still to be improved.

CRediT authorship contribution statement

Ruggero Forte: Conceptualization, Methodology, Investigation, Writing - original draft. **Pierluigi Chiovaro:** Conceptualization, Methodology, Investigation, Writing - original draft. **Pietro Alessandro Di Maio:** Conceptualization, Methodology, Writing - review & editing, Supervision. **Nasr Ghoniem:** Conceptualization, Methodology, Writing - review & editing, Supervision.

Declaration of competing interest

The authors declare that they have no known competing financial interests or personal relationships that could have appeared to influence the work reported in this paper.

Disclaimer

This work has been carried out within the framework of the EUROfusion consortium and has received funding from the Euratom research and training programme 2014–2018 and 2019–2020 under grant agreement No 633053.

The views and opinions expressed herein do not necessarily reflect those of the European Commission.

Table A.1
Results obtained from the optimization campaign. The optimum point obtained is highlighted in bold.

Run	X_{start}	$f(X_{start})$	X_{end}	$f(X_{end})$
#1	$\begin{pmatrix} 6 & 14.000 & 7.000 & 7.000 \\ 6 & 12.087 & 5.697 & 13.378 \\ 6 & 10.156 & 8.895 & 12.587 \\ 7 & 10.316 & 9.106 & 9.774 \\ 6 & 9.705 & 9.458 & 11.122 \\ 5 & 9.163 & 7.237 & 8.194 \\ 6 & 13.486 & 6.438 & 9.567 \\ 6 & 14.300 & 6.145 & 10.721 \end{pmatrix}$	$\begin{pmatrix} 5.945 \\ 4.397 \\ 3.344 \\ 3.488 \\ 3.356 \\ 5.037 \\ 5.164 \\ 5.139 \end{pmatrix}$	$\begin{pmatrix} 6 & 6.898 & 12.296 & 17.027 \\ 6 & 6.824 & 12.304 & 17.059 \\ 6 & 6.887 & 12.162 & 17.323 \\ 6 & 6.798 & 12.379 & 17.027 \\ 6 & 6.836 & 12.319 & 16.956 \\ 6 & 6.851 & 12.340 & 17.019 \\ 6 & 6.852 & 12.196 & 17.040 \\ 6 & 6.778 & 12.402 & 16.884 \end{pmatrix}$	$\begin{pmatrix} 2.060 \\ 2.045 \\ 2.054 \\ 2.037 \\ 2.051 \\ 2.049 \\ 2.058 \\ 2.038 \end{pmatrix}$
#2	$\begin{pmatrix} 6 & 14.000 & 7.000 & 7.000 \\ 6 & 14.013 & 6.993 & 6.999 \\ 6 & 11.176 & 7.268 & 6.281 \\ 7 & 9.057 & 11.442 & 6.017 \\ 5 & 13.596 & 6.315 & 18.846 \\ 6 & 13.420 & 7.863 & 11.435 \\ 7 & 9.796 & 7.580 & 9.744 \\ 6 & 13.468 & 6.939 & 11.020 \end{pmatrix}$	$\begin{pmatrix} 5.945 \\ 5.951 \\ 5.679 \\ 3.720 \\ 4.171 \\ 4.304 \\ 3.722 \\ 4.637 \end{pmatrix}$	$\begin{pmatrix} 5 & 6.242 & 15.081 & 14.680 \\ 5 & 6.052 & 15.063 & 13.961 \\ 5 & 6.189 & 15.214 & 14.065 \\ 5 & 6.158 & 15.127 & 13.890 \\ 5 & 6.113 & 15.021 & 14.095 \\ 5 & 6.254 & 15.210 & 14.338 \\ 5 & 6.160 & 15.239 & 13.873 \\ 5 & 6.236 & 15.118 & 14.179 \end{pmatrix}$	$\begin{pmatrix} 2.044 \\ 2.056 \\ 2.065 \\ 2.076 \\ 2.061 \\ 2.059 \\ 2.071 \\ 2.072 \end{pmatrix}$
#3	$\begin{pmatrix} 6 & 14.000 & 7.000 & 7.000 \\ 5 & 6.578 & 14.527 & 12.805 \\ 8 & 9.531 & 8.777 & 6.392 \\ 5 & 8.906 & 10.097 & 6.387 \\ 7 & 9.153 & 11.437 & 9.664 \\ 7 & 11.702 & 8.983 & 9.751 \\ 9 & 10.241 & 5.287 & 9.366 \\ 7 & 12.254 & 8.088 & 10.620 \end{pmatrix}$	$\begin{pmatrix} 5.945 \\ 2.275 \\ 3.963 \\ 4.715 \\ 2.963 \\ 3.767 \\ 4.117 \\ 3.902 \end{pmatrix}$	$\begin{pmatrix} 5 & 6.310 & 15.147 & 14.481 \\ 5 & 6.277 & 15.178 & 13.951 \\ 5 & 6.130 & 15.405 & 13.390 \\ 5 & 6.180 & 15.340 & 13.663 \\ 5 & 6.284 & 15.251 & 14.122 \\ 5 & 6.231 & 15.284 & 13.697 \\ 5 & 6.360 & 15.079 & 14.432 \\ 5 & 6.232 & 15.459 & 13.557 \end{pmatrix}$	$\begin{pmatrix} 2.064 \\ 2.091 \\ 2.088 \\ 2.082 \\ 2.076 \\ 2.093 \\ 2.081 \\ 2.092 \end{pmatrix}$
#4	$\begin{pmatrix} 6 & 14.000 & 7.000 & 7.000 \\ 7 & 11.218 & 10.170 & 6.782 \\ 7 & 10.467 & 10.248 & 7.732 \\ 5 & 11.362 & 5.821 & 22.833 \\ 6 & 12.608 & 8.748 & 8.780 \\ 7 & 9.656 & 10.353 & 9.306 \\ 5 & 10.626 & 7.547 & 13.069 \\ 7 & 12.891 & 7.838 & 10.745 \end{pmatrix}$	$\begin{pmatrix} 5.945 \\ 4.112 \\ 3.709 \\ 3.590 \\ 4.465 \\ 3.245 \\ 3.967 \\ 4.052 \end{pmatrix}$	$\begin{pmatrix} 8 & 8.054 & 9.537 & 12.800 \\ 8 & 8.048 & 9.523 & 12.904 \\ 8 & 8.080 & 9.704 & 13.024 \\ 8 & 8.027 & 9.699 & 12.750 \\ 8 & 8.031 & 9.684 & 12.810 \\ 8 & 8.065 & 9.523 & 13.014 \\ 8 & 8.011 & 9.769 & 12.737 \\ 8 & 8.043 & 9.588 & 12.780 \end{pmatrix}$	$\begin{pmatrix} 2.500 \\ 2.492 \\ 2.470 \\ 2.482 \\ 2.480 \\ 2.487 \\ 2.473 \\ 2.494 \end{pmatrix}$
#5	$\begin{pmatrix} 6 & 14.000 & 7.000 & 7.000 \\ 8 & 11.553 & 6.405 & 6.795 \\ 6 & 11.569 & 5.717 & 8.790 \\ 8 & 9.615 & 8.323 & 9.927 \\ 7 & 10.422 & 6.638 & 9.725 \\ 10 & 15.341 & 4.575 & 8.458 \\ 7 & 12.286 & 7.591 & 9.880 \\ 5 & 12.719 & 4.165 & 11.903 \end{pmatrix}$	$\begin{pmatrix} 5.945 \\ 4.977 \\ 5.423 \\ 3.271 \\ 4.115 \\ 5.391 \\ 4.148 \\ 6.353 \end{pmatrix}$	$\begin{pmatrix} 5 & 6.351 & 13.395 & 20.664 \\ 5 & 6.231 & 13.058 & 20.339 \\ 5 & 6.378 & 13.160 & 21.069 \\ 5 & 6.254 & 13.708 & 19.693 \\ 5 & 6.250 & 13.704 & 19.744 \\ 5 & 6.227 & 14.547 & 17.902 \\ \mathbf{5} & \mathbf{6.194} & \mathbf{13.744} & \mathbf{19.497} \\ 5 & 6.399 & 12.840 & 21.624 \end{pmatrix}$	$\begin{pmatrix} 1.887 \\ 1.895 \\ 1.891 \\ 1.887 \\ 1.884 \\ 1.908 \\ \mathbf{1.881} \\ 1.894 \end{pmatrix}$

Appendix. Results of the optimization campaign

Table A.1 show the evolution of the complex from the start to the end of each optimization run. In particular, $\mathbf{X}_{start}$ and $\mathbf{X}_{end}$ represent the initial and the final complexes, respectively, defined as arrays with $n = 4$ columns by $k = 2n$ rows, wherein each row (N, R, a, b) represents a point of the complex, whereas $f(\mathbf{X}_{start})$ and $f(\mathbf{X}_{end})$ are the arrays containing the respective objective function values.

As shown in the table, Runs #1, #2 and #3 ended almost to the same objective function value (2.04÷2.09), although the first run got that value with a different variables combination. Hence, the results of the first three runs said that, considering all the constraints, a potential global minimum of the objective function is located around those values.

Conversely, Run #4 finished with an higher objective function value, meaning that the complex got stuck in a local minimum and could not proceed towards the global one. As stated above, this event can happen using the Complex method when lots of constraints are imposed.

Finally, the Run #5 ended almost with the same combination of variables of Runs #2 and #3 (i.e. $N = 5$, $R \approx 6.2$ mm), but was able to reach a lower value of the objective function (≈ 1.90) by means of a slight different combination of the channels' dimension a and b.

References

[1] G. Federici, et al., Overview of the DEMO staged design approach in Europe, Nucl. Fusion 58 (066013) (2019) http://dx.doi.org/10.1088/1741-4326/ab1178.

[2] M. Box, A new method of constrained optimization and a comparison with other method, Comput. J. 8 (1) (1965) 42–52.

[3] MATLAB, (R2015b), The MathWorks Inc., Natick, Massachusetts, USA.

[4] COMSOL Multiphysics, COMSOL AB, Stockholm, Sweden.

[5] H. Tanigawa, et al., Status and key issues of reduced activation ferritic/martensitic steels as the structural material for a DEMO blanket, J. Nucl. Mater. 417 (2011) 9–15, http://dx.doi.org/10.1016/j.jnucmat.2011.05.023.

[6] A.D. Nevo, et al., Recent progress in developing a feasible and integrated conceptual design of the WCLL BB in EUROfusion project, Fusion Eng. Des. 146 (B) (2019) 1805–1809, http://dx.doi.org/10.1016/j.fusengdes.2019.03.040.

[7] F. Edemetti, et al., Thermal-hydraulic analysis of the DEMO WCLL elementary cell: BZ tubes layout optimization, Fusion Eng. Des. 160 (111956) (2020) http://dx.doi.org/10.1016/j.fusengdes.2020.111956.

[8] F. Edemetti, et al., Optimization of the first wall cooling system for the DEMO WCLL blanket, Fusion Eng. Des. 161 (111903) (2020) http://dx.doi.org/10.1016/j.fusengdes.2020.111903.

[9] R. Forte, et al., Preliminary design of the top cap of DEMO Water-Cooled Lithium Lead breeding blanket segments, Fusion Eng. Des. 161 (111884) (2020) http://dx.doi.org/10.1016/j.fusengdes.2020.111884.

[10] I. Catanzaro, et al., Parametric study of the influence of double-walled tubes layout on the DEMO WCLL breeding blanket thermal performances, Fusion Eng. Des. 161 (111893) (2020) http://dx.doi.org/10.1016/j.fusengdes.2020.111893.

[11] F. Moro, et al., Nuclear analysis of the water cooled lithium lead DEMO reactor, Fusion Eng. Des. 160 (2020) http://dx.doi.org/10.1016/j.fusengdes.2020.111833.

[12] U. Fuscher, et al., Required, achievable and target TBR for the European DEMO, Fusion Eng. Des. 155 (111553) (2020) http://dx.doi.org/10.1016/j.fusengdes.2020.111553.

[13] RCC-MRx, Design and Construction Rules for Mechanical Components of Nuclear Installations, AFCEN, 2012.

[14] J. Nelder, R. Mead, A simplex method for function minimization, Comput. J. 7 (1965) 308–313.

[15] J. Guin, Modification of the Complex method of constraint optimization, Comput. J. 10 (1968) 416–417.

[16] P. Krus, Optimization based on simulation for design of fluid power systems, in: Proceedings of ASME Winter Annual Meeting, Anaheim, USA, 1992.

[17] J. Andersson, Multiobjective Optimization in Engineering Design: Applications to Fluid Power Systems (Doctoral Thesis), Linköpings Universitet, Sweden, 2001.

[18] N.K. Sahoo, et al., Modified complex method for constrained design and optimization of optical multilayer thin-film devices, Appl. Phys. A 59 (1994) 317–326.

[19] M.I. Haque, et al., Optimal frame design with discrete members using the complex method, Comput. Struct. 59 (1996) 847–858.

[20] F. Gillemot, et al., Material Property Handbook Pilot Project on EUROFER97, Tech. rep., 2016.

[21] ITER SDC-IC, Appendix A, Materials Design Limit Data, ITER IDM, Ref.:ITER_D_222RLN, 2013.

[22] D. Martelli, et al., Literature review of lead-lithium thermophysical properties, Fusion Eng. Des. 138 (2019) 183–195, http://dx.doi.org/10.1016/j.fusengdes.2018.11.028.

[23] A.D. Nevo, et al., WCLL BB Design and Integration Studies 2019 Activities, Tech. Rep. EUROfusion IDM Ref.:EFDA_D_2P5NE5, 2019.

[24] P.D. Maio, et al., On the thermo-mechanical behaviour of DEMO water-cooled lithium lead equatorial outboard blanket module, Fusion Eng. Des. 124 (2017) 725–729, http://dx.doi.org/10.1016/j.fusengdes.2017.05.051.

[25] P. Chiovaro, Neutronics: Design & analyses, in: Presentation at the WCLL BB Design Review Meeting 2019, 2019.

[26] P. Chiovaro, et al., Parametric study of the influence of First Wall cooling water on the Water Cooled Lithium Lead Breeding Blanket nuclear response, Fusion Eng. Des. 146 (B) (2019) 2070–2073, http://dx.doi.org/10.1016/j.fusengdes.2019.03.105.

[27] F. Incropera, Fundamentals of Heat and Mass Transfer, John Wiley & Sons Inc., 1985.

[28] Y. Huang, et al., Thermo-structural design of the European DEMO water-cooled blanket with a multiscale-multiphysics framework, Fusion Eng. Des. 135 (A) (2018) 31–41, http://dx.doi.org/10.1016/j.fusengdes.2018.07.007.

[29] J. Aubert, et al., Design and preliminary analyses of the new Water Cooled Lithium Lead TBM for ITER, Fusion Eng. Des. 160 (111921) (2020) http://dx.doi.org/10.1016/j.fusengdes.2020.111921.

[30] X-5 Monte Carlo Team, MCNP—A General Monte Carlo N-Particle Transport Code, Version 5, LANL, Los Alamos, New Mexico, USA, 2003.

[31] JEFF3.2 Nuclear Data Library, 2008, http://www.oecd-nea.org/.

[32] G. Spagnuolo, et al., A multi-physics integrated approach to breeding blanket modelling and design, Fusion Eng. Des. 143 (2019) 35–40, http://dx.doi.org/10.1016/j.fusengdes.2019.03.131.

[33] R. Favetti, et al., Validation of multi-physics integrated procedure for the HCPB breeding blanket, Int. J. Comput. Methods 17 (6) (2020) http://dx.doi.org/10.1142/S0219876219500099.

[34] D. She, On the white boundary condition in Monte Carlo simulation, Ann. Nucl. Energy 132 (2019) 413–414, http://dx.doi.org/10.1016/j.anucene.2019.05.006.

[35] G.A. Spagnuolo, Integrated Multi-Physics Design Tool for Fusion Breeding Blanket Systems - Development and Validation (Doctoral Thesis), Karlsruher Institut für Technologie (KIT), 2020, http://dx.doi.org/10.5445/IR/1000123701.

[36] E. Gaganidze, et al., Assessment of neutron irradiation effects on RAFM steels, Fusion Eng. Des. 88 (3) (2013) 118–128, http://dx.doi.org/10.1016/j.fusengdes.2012.11.020.